CHAPTER 185

A numerical simulation of beach evolution based on a nonlinear dispersive wave-current model

Shinji Sato[1] and Michael B. Kabiling[2]

ABSTRACT

A numerical wave model based on the Boussinesq equation was extended to the computation of two-dimensional wave-current field including diffraction, refraction and wave breaking. The energy dissipation due to wave breaking was modeled by a momentum mixing term using eddy viscosity. Beach deformation was estimated based on the wave-current field simulated in the nearshore region. Energetics-based equations were used to estimate the total sediment transport in the cross-shore and longshore directions. The model applicability was confirmed with laboratory experiments.

1. INTRODUCTION

In the nearshore region, where water depths are shallow and amplitudes are relatively large, waves are highly nonlinear characterized by asymmetric orbital motion of the water particle. This nonlinearity becomes increasingly dominant with decreasing water depth. Hence, it is expected that numerical models based on the linear wave theory will not provide an accurate simulation of the nearshore wave phenomenon. Moreover, since the nearshore current is caused by the gradient of nonlinear radiation stress, it cannot be estimated simultaneously with the wave variables in linear wave models.

The Boussinesq equation can be considered as one of the valid nonlinear dispersive wave theories for finite amplitude wave transformation. The nearshore currents generated by the wave action can also be determined from nonlinear wave computation using the Boussinesq equations. The performance of the Boussinesq equations in 1-D wave transformation was evaluated by Madsen and Warren (1984)[10], Abbott *et al.* (1984)[1], and McCowan (1987)[13]. It was noted that Boussinesq equations with various forms of the dispersion terms generally performed well in the shallow water region. Madsen *et al.* (1991)[11] also presented a method of extending the validity of the Boussinesq equations to deeper water. The use of the Boussinesq equations was extended to the surf zone by more recent researches by Schäffer *et al.* (1992)[16], Karambas *et al.* (1992)[8] and Sato *et al.*

[1] Dr. Eng., Coastal Engineering Division, Public Works Research Institute, Ministry of Construction, 1 Asahi, Tsukuba, 305, JAPAN

[2] Dr. Eng., MBK Engineering, 444 Jupiter St., San Fernando Subdivision, San Fernando, Pampanga, 2000, PHILIPPINES

(1992)[15]. It was shown that with the use of an appropriate additional term expressing the momentum mixing due to wave breaking, the Boussinesq equations give reasonable results even inside the surf zone. However, most of the previous works in this area have been confined to 1-D wave modeling.

In this study, the nonlinear dispersive wave model based on the Boussinesq equation is extended for wave transformation in two horizontal dimensions. A new breaking criterion using the ratio of the water particle velocity at the crest surface to the wave celerity for three-dimensional wave field is presented. A momentum mixing term is introduced to simulate the energy dissipation due to wave breaking and thus extend the use of the Boussinesq equations into the surf zone. These two factors extended the wave-current model application into the surf zone. A beach run-up sub-model similar to that used by Iwasaki and Mano (1979)[5] was added to extend the model application up to the swash zone. It also allowed for the estimation of the beach deformation beyond the initial shoreline. Results from the numerical computations are compared with previous theoretical works and with existing laboratory data.

2. WAVE AND CURRENT MODELING

2.1. Governing equations

The Boussinesq equations for 2-D incompressible flow applicable for a horizontal or mildly sloping bottom are used as the basis for the governing equations. Additional momentum mixing terms M_{Dx} and M_{Dy} were added into the Boussinesq equations to simulate the energy dissipation due to wave breaking inside the surf zone. Another term was also added to include the effect of the bottom friction. The governing equations thus read:

$$\frac{\partial \eta}{\partial t}+\frac{\partial Q_x}{\partial x}+\frac{\partial Q_y}{\partial y}=0 \tag{1}$$

$$\frac{\partial Q_x}{\partial t}+\frac{\partial}{\partial x}\left(\frac{Q_x^2}{d}\right)+\frac{\partial}{\partial y}\left(\frac{Q_x Q_y}{d}\right)+g d\frac{\partial \eta}{\partial x} =\frac{1}{3}h^2\left(\frac{\partial^3 Q_x}{\partial x^2 \partial t}+\frac{\partial^3 Q_y}{\partial x \partial y \partial t}\right)-\frac{f_w}{2d^2}Q_x\sqrt{Q_x^2+Q_y^2}+M_{Dx} \tag{2}$$

$$\frac{\partial Q_y}{\partial t}+\frac{\partial}{\partial x}\left(\frac{Q_x Q_y}{d}\right)+\frac{\partial}{\partial y}\left(\frac{Q_y^2}{d}\right)+g d\frac{\partial \eta}{\partial y} =\frac{1}{3}h^2\left(\frac{\partial^3 Q_x}{\partial x \partial y \partial t}+\frac{\partial^3 Q_y}{\partial y^2 \partial t}\right)-\frac{f_w}{2d^2}Q_y\sqrt{Q_x^2+Q_y^2}+M_{Dy} \tag{3}$$

where as shown in Fig. I, $Q_x(x,y,t)=\bar{u}_x d$ and $Q_y(x,y,t)=\bar{u}_y d$ are the depth-integrated flow rates in the x-axis and y-axis directions respectively, $\bar{u}_x=\bar{u}_x(x,y,t)$ and $\bar{u}_y=\bar{u}_y(x,y,t)$ are the depth-averaged water particle velocities in the x-axis and y-axis directions respectively, $d(=h+\eta)$ is the total water depth, $h=h(x,y)$ is the still water depth, $\eta=\eta(x,y,t)$ is the water surface elevation, g is the acceleration due to gravity, f_w is the bottom friction coefficient, and M_{Dx} and M_{Dy} are the momentum correction terms in the x-axis and y-axis directions respectively.

An Alternating Direction Implicit (ADI) finite difference scheme with a double sweep algorithm on a staggered rectangular grid region was used in the wave-current computations. In all

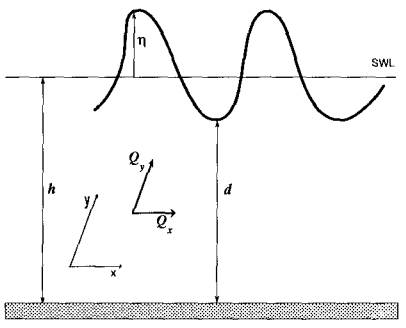

Figure 1 Definition sketch of a typical wave profile.

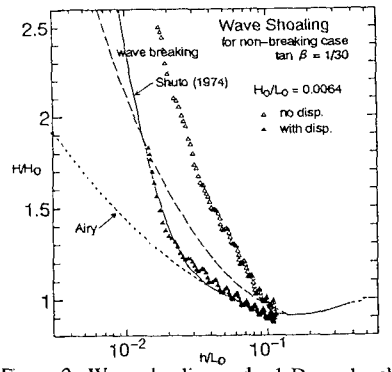

Figure 2 Wave shoaling under 1-D non-breaking wave computations.

computations, monochromatic first-order cnoidal waves were generated at the incident boundary. The incident boundary was set as an absorbing boundary which allowed the reflected waves to pass through freely. An absorbing boundary was defined by solving the radiation problem along this boundary. The computation started from still water and continued until both wave and current fields reached equilibrium state. The time required to reach the equilibrium was about 40 wave periods in the present computations.

2.2. Wave shoaling

To verify the numerical scheme, 1-D non-breaking wave computations ($M_{Dx} = M_{Dy} = 0$) were performed on a rectangular region where the onshore boundary was set as an absorbing boundary which allowed the non-breaking waves to pass through freely. The still water depths at the incident and onshore boundaries were set to $0.12L_o$ and to just below the wave breaking limit respectively. Numerical computations for bottom slope $\tan\beta = 1/30$ to $1/20$ were made with incident wave condition $H_o/L_o = 0.0064$ where H_o and L_o are the deep water wave height and wavelength respectively.

Figure 2 shows the ratio of the wave height to the deep water wave height H/H_o for computations with and without the dispersion terms. The small undulations were caused by small amounts of wave reflection arising from the bottom slope as well as the onshore boundary. The values of H/H_o from nonlinear non-dispersive wave computations overestimate wave shoaling. In contrast, those from nonlinear dispersive wave computations adhere closely to the theoretical curve presented by Shuto (1974)[17]. This indicates the importance of including the dispersion terms in nonlinear wave computations. These results confirmed the capability of the Boussinesq wave model for wave shoaling up to the breaking limit.

2.3. Two-dimensional wave breaking criterion

In order to establish an appropriate 2-D wave breaking criterion for nonlinear dispersive waves in a multi-directional wave field, the ratio of the water particle horizontal velocity at the surface of wave crest u_{smax} to the wave celerity c at the breaking point was investigated. The aim of the investigation is to determine the critical ratio at incipient wave breaking.

The wave celerity c was taken to be equal to the celerity in the direction of the maximum horizontal water particle velocity u_{smax} which occurs at the crest surface. The ratio u_{smax}/c was thus

estimated by:

$$\frac{u_{smax}}{c} = \frac{\left|\vec{k} \cdot \vec{u}_{smax}\right|}{\sigma} \tag{4}$$

where $\vec{k}$ is the wave number vector and σ is the angular frequency. The wave number $\vec{k}$ was determined from the gradient of the phase lag Φ. The phase lag was estimated from the Fourier analysis of the computed water surface elevation $\eta(t)$. A quadratic vertical distribution of the horizontal velocity was assumed. Based on the investigation, the critical values of u_{smax}/c was found to be in the range $0.4 \le u_{smax}/c \le 0.70$ depending on the bottom slope and incident wave condition.

2.4. Energy dissipation due to wave breaking

Significant amount of energy is dissipated by the turbulence generated by the breaking of waves. Several momentum correction models have been proposed so far to simulate wave damping in the surf zone (*e.g.*,Karambas and Koutitas, 1992, Schäffer *et al.*, 1992). Watanabe and Dibajnia (1988)[21] presented a numerical wave model based on the linear wave theory. It computes wave transformation by using a set of time-dependent mass and momentum conservation equations that are equivalent to the mild-slope equations. The functional form of M_D that was used in the wave transformation computations from this linear wave model for which results well agree with laboratory data is:

$$M_D = -f_D \cdot Q = -\alpha_D \tan\beta \sqrt{\left(\frac{g}{\bar{d}}\right)\left(\frac{\hat{Q}-Q_r}{Q_s-Q_r}\right)} \cdot Q \tag{5}$$

where f_D is an energy dissipation coefficient, Q is the discharge per unit width, α_D is a coefficient which is 2.5 inside the surf zone and zero elsewhere, $\tan\beta$ is the bottom slope, $\bar{d}$ is the mean total depth, $\hat{Q}$ is the amplitude of discharge per unit width, Q_s is the wave induced flow rate inside the surf zone, and Q_r is the flow rate amplitude of recovered waves. Based on the experimental data of Isobe (1986)[4] and Maruyama and Shimizu (1986)[12] respectively, Q_s and Q_r can be estimated as:

$$Q_s = 0.4\left(0.57 + 5.3\tan\beta\right)\sqrt{g\bar{d}^3} \tag{6a}$$

$$Q_r = 0.135\sqrt{g\bar{d}^3} \tag{6b}$$

Wave breaking however, involves strong turbulence and momentum mixing particularly at the front face of the wave. The energy dissipation is a direct result of the diffusion of momentum in the surf zone. It is therefore necessary to use a more appropriate form of M_D that can better describe these phenomena. Sato *et al.* (1992)[15] presented an energy dissipation term that was proportional to the diffusion of the momentum. The following formulation of M_{Dx} and M_{Dy} by Sato *et al.* (1992) in terms of an eddy viscosity ν_B was used to describe the momentum exchange due to turbulence.

$$M_{Dx} = \nu_e\left(\frac{\partial^2 Q_x}{\partial x^2} + \frac{\partial^2 Q_x}{\partial y^2}\right) \tag{7a}$$

$$M_{Dy} = \nu_e\left(\frac{\partial^2 Q_y}{\partial x^2} + \frac{\partial^2 Q_y}{\partial y^2}\right) \quad \text{with} \quad \nu_e = \nu_B + \nu_L \tag{7b}$$

The functional form of ν_B was analogically deduced from Eq. (5). By assuming sinusoidally varying Q, the form of ν_B for long waves becomes:

$$\nu_B = \frac{\alpha_D\, g\, \bar{d}\tan\beta}{\sigma^2}\sqrt{\left(\frac{g}{\bar{d}}\right)\left(\frac{\hat{Q}-Q_r}{Q_s-Q_r}\right)} \tag{8}$$

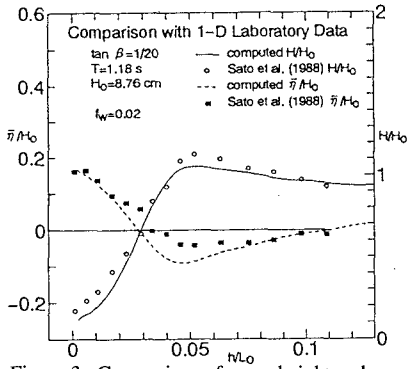

Figure 3 Comparison of wave height and mean water surface.

The form of ν_B in Eq. (8) is consistent with Eq. (5). Sato *et al.* (1992) confirmed that the momentum mixing model given by Eq. (8) is capable of simulating the tilting of the wave profile as the wave propagates into shallow water.

Equation (8) is used only in the surf zone and the eddy viscosity ν_B is zero outside the surf zone. However, this will result in the appearance of enormously large velocities at sharp corners of structures located outside the surf zone. These large velocities occur in places where there is a sudden difference in wave height and mean water level. They are likely to occur in sharp corners like at the tip of a detached breakwater. To avoid these large velocities, additional viscosity is introduced. An appropriate form for this additional viscosity ν_L is found to be similar to that proposed by Longuet-Higgins (1970)[9] and is given by

$$\nu_L = 0.016\, l \tan\beta \sqrt{g\,\bar{d}} \tag{9}$$

where l is the horizontal distance from the shoreline. The magnitude of ν_L is set to be much smaller than ν_B so as not to cause additional wave damping.

2.5. One-dimensional wave transformation

Data from a series of 1-D laboratory experiments conducted in a wave flume by Sato *et al.* (1988)[14] were used to verify the wave transformation capability of the present model in the surf zone. In one wave flume experiment, the instantaneous surface elevation and the near-bottom velocity at several points were measured along a line in the direction of the wave propagation. The bottom slope was $\tan\beta = 1/20$, the still water depth at the incident boundary $h_i = 40$ cm, the monochromatic incident wave period $T = 1.18$ s and the incident wave height $H_o = 8.76$ cm.

The computed non-breaking wave heights as well as the mean water level $\bar{\eta}$ well agree with the measurements as shown in Fig. 3. With the inclusion of the momentum mixing terms into the Boussinesq equations, the computed H/H_o in the surf zone also agree well with the measured H/H_o. From the profile of $\bar{\eta}/H_o$, it can be seen that the model is capable of simulating the wave set-down before wave breaking and the subsequent wave set-up after wave breaking.

The computed instantaneous water surface elevation $\eta(t/T)$ and near-bottom velocity $u_b(t/T)$ were compared with the measurements. Figures 4(a) and 4(b) show η and u_b respectively at two measuring points located before and after wave breaking. In these figures, t denotes the time within one wave period and x is the horizontal distance from the still water shoreline.

The best agreement between computation and measurement seems to occur before wave breaking. This is expected since the Boussinesq theory has been proven to be a valid nonlinear wave theory for non-breaking water waves. Inside the surf zone, there is a good agreement of the computed η with the data. The computed near-bottom velocity u_b also agrees fairly with the data. The slight deterioration in model accuracy in the surf zone may be due to three reasons. First, the Boussinesq theory may not be valid for such strongly nonlinear dispersive waves where wave nonlinearity and wave dispersion do not have the same order of magnitude. Second, strong turbulent mixing generated by wave breaking cannot be well simulated by the simple eddy viscosity approach that uses a constant

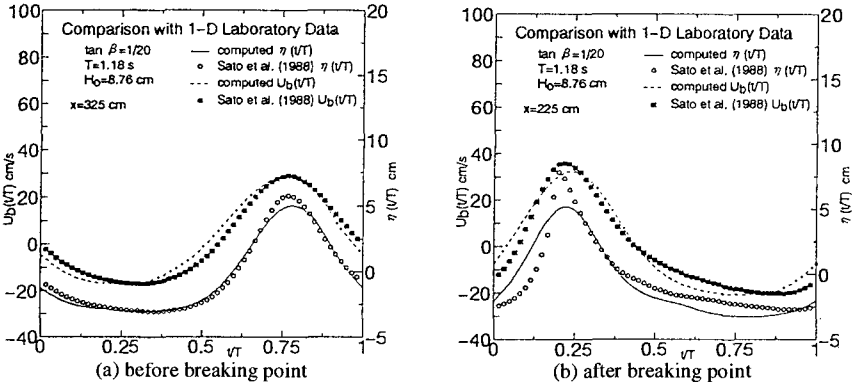

Figure 4 Time history of water surface elevation $\eta(t/T)$ and near-bottom velocity $u_b(t/T)$.

eddy viscosity value for one wave period. Third, the assumption of a nearly horizontal slope may have caused this inaccuracy. In spite of these, the model can be regarded to be applicable in the region outside the surf zone and fairly accurate within the surf zone.

3. BEACH DEFORMATION MODELING

3.1. Total sediment transport equations

Two sediment transport equations were used by Kabiling and Sato (1993)[7] in modeling 3-D beach deformation. The first of which was used to simulate the sediment transport due to the current. It can be expected therefore that cross-shore sediment transport will not be simulated. On the other hand, the second model based on the Bailard (1981)[2] equations, was seen to be inaccurate around the breaking point. To improve the accuracy in estimating sediment transport around the breaking point and at the same time to include the sediment transport due to asymmetric oscillatory motion of nonlinear waves during one wave period, another set of energetics-based sediment transport equations is needed.

The bed load and suspended sediment equations were formulated to include a threshold value for the initiation of sediment transport. In the case of bed load transport, this threshold value can include the effect of wave breaking on the bed load transport. The bed load transport $\vec{q}_B(t)$ at any time t was formulated as:

$$\frac{\vec{q}_B(t)}{\sqrt{(\rho_s/\rho-1)\,g\,D_s^3}} = \alpha_B \left|\Psi(t)\right|^a \left[\max\left(\Psi(t)-\Psi_c,0\right)\right]^b \cdot \frac{\vec{u}_b(t)}{\left|\vec{u}_b(t)\right|} \tag{10a}$$

where α_B, a and b are parameters that need calibration, Ψ_c is the critical Shield's parameter for the initiation of bed load transport, $\vec{u}_b(t)$ is the near-bottom velocity at time t, ρ_s is the density of the sediment particle, and ρ is the density of water.

Investigations by Kabiling and Sato (1993) on their second sediment transport model based on Bailard (1981) equations revealed that the overestimation of the total sediment transport at the breaking point was mainly coming from the estimation of the suspended sediment transport which was modeled in terms of the near-bottom velocity raised to the fifth power. This can be corrected by

expressing suspended sediment transport as a function of near-bottom velocity raised to less than the fifth power. Furthermore, it was revealed that the first sediment transport model by Kabiling and Sato (1993) was able to simulate the suspended sediment transport. This leads one to adopt a form for the present suspended sediment transport equation in the form:

$$\frac{\vec{q}_S(t)}{w_s D_s} = \alpha_s \left[\max\left(\Psi(t) - \Psi_c, 0\right)\right]^p \cdot \frac{\vec{u}_b(t)}{\left|\vec{u}_b(t)\right|} \tag{10b}$$

where $\vec{q}_S(t)$ is the suspended sediment transport rate, w_s is the sediment particle fall velocity, and α_S and p are parameters that also need calibration. Equation (10b) is different from the second sediment transport by Kabiling and Sato (1993) since it is expressed as a function of the instantaneous near-bottom velocity. This will result in the inclusion of the effect of nonlinear waves on the suspended sediment transport. In both Eqs. (10a) and (10b), the Shield's parameter is estimated using the Jonsson (1966)[6] friction coefficient:

$$\Psi(t) = \frac{f_w}{2} \frac{\left[\vec{u}_b(t)\right]^2}{\left(\rho_s/\rho - 1\right) g D_s} \tag{11}$$

The total sediment transport in the present model is estimated by the summation of Eqs. (10a) and (10b). Sediment transport rate in the swash zone was overestimated due to the large velocity moments from highly nonlinear waves that are usually found in this zone. The direction of the net sediment transport was also seen to have been always in the offshore direction which indicated that the offshore rush was larger than the onshore rush. This may he due to the big difference in the water depth during onshore and offshore rushing of the shoreline. During the offshore rush, total water depth is less than that during the onshore rush so larger velocities will result during the offshore rush. In order to avoid unrealistic erosion, sediment transport rate in the swash zone was linearly interpolated between the sediment transport at the still water shoreline and the zero sediment transport at the maximum beach run-up point.

To calculate the local bottom elevation change due to the sediment transport, the sediment conservation equation proposed by Watanabe *et al.* (1986) is used. The sediment conservation equation is given by

$$\frac{\partial h}{\partial t} = -\frac{\partial z}{\partial t} = \frac{1}{1-\lambda_v}\left\{\nabla \cdot \left(\vec{\bar{q}} + \varepsilon \left|\vec{\bar{q}}\right| \nabla \cdot h\right)\right\} \tag{12}$$

where z is the bottom elevation, λ_v (=0.4) the sediment porosity, and ε is a coefficient that reflects the effect of local bottom slope on the sediment transport.

3.2. Two-dimensional beach deformation

Watanabe *et al.* (1980)[19] measured the change in beach topography in a wave flume. In one set of the experiments, the initial bed slope was $\tan\beta = 1/20$ and the sediment mean diameters were $D_s = 0.2$ and 0.7 mm respectively. Monochromatic incident wave periods were 1.0, 1.5, and 2.0 s while wave steepness varied from 0.006 to 0.073. The beach was exposed to wave action for a period of one hour. At the end of this period, the beach profile was measured and the cross-shore sediment transport rate was computed based on the measured beach deformation.

One-dimensional wave computations for six cases were done. Based on the computed velocity field, Eqs. (10a) and (10b) with Eq. (12) were used to estimate the beach deformation for each case. The values of the parameters in Eqs. (10a) and (10b) were $\alpha_B = 1.0$, $a = 0.5$, $b = 1.0$, $\alpha_s = 3.5$, $p = 1.0$, and $\Psi_c = 0$. Since surf zone beach deformation is of prime interest in the present study, the

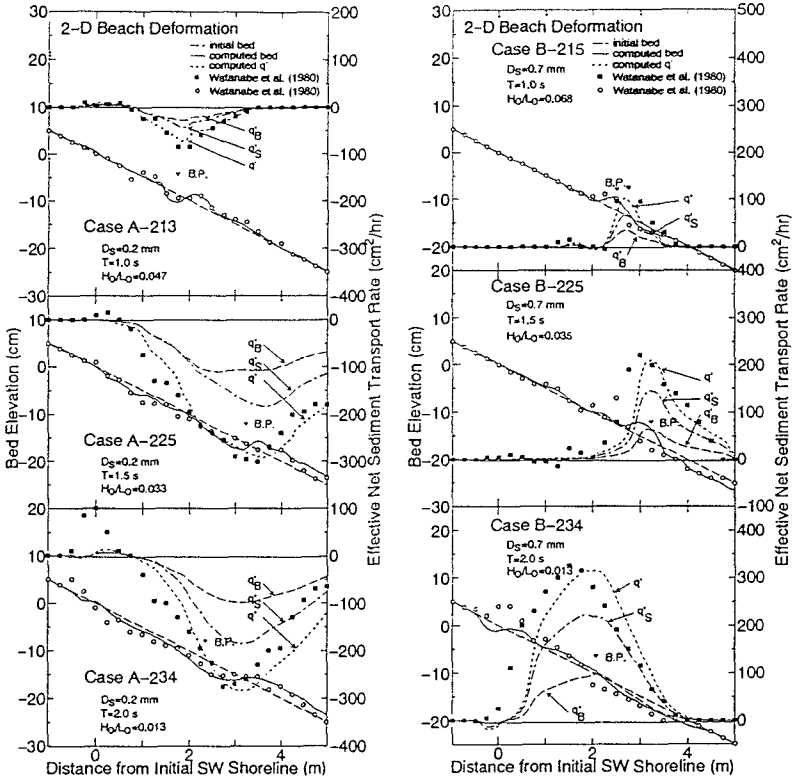

(a) $D_s = 0.2$ mm (b) $D_s = 0.7$ mm

Figure 5 Computed bed elevations and cross-shore effective net sediment transport rates.

values of a and b were such as to make the bed load proportional to u_b^3. The beach deformation time step $\Delta t'_e$ was estimated following Watanabe *et al.* (1986):

$$\Delta t'_e \le \min\left\{\frac{1}{2}\frac{\Delta x^2}{\varepsilon|\overline{q}_x|_{max}}, \frac{1}{2}\frac{\Delta y^2}{\varepsilon|\overline{q}_y|_{max}}\right\} \tag{13}$$

where Δx and Δy are the grid spacing in the x-axis and y-axis respectively, $\overline{q}_x$ and $\overline{q}_y$ are the net total sediment transport rates in the x-axis and y-axis respectively and $\varepsilon = 4.0$.

(1) Fine Sediment

Figure 5(a) shows the computed bed elevation, cross-shore net bed load q'_B, suspended sediment q'_S, and total sediment q' transport rates (which are positive in the onshore direction) for $D_s = 0.2$ mm and $\tan\beta = 1/20$ (Cases A-213, A-225 and A-234). The closed triangle indicates the computed location of the breaking point. When compared with the measured beach topography (open circle) and computed net sediment transport rate (closed square) of Watanabe *et al.* (1980), the

magnitude of the computed beach deformation and sediment transport rates have the same order of magnitude. This confirmed the values of the parameters used in Eqs. (10a) and (10b).

The direction of the sediment transport as computed by Watanabe *et al.* (1980) was generally offshore. Sand ripples were observed during the experiment which indicated the predominance of suspended sediments. The direction of sediment transport was simulated correctly by the present model with suspended sediment transport accounting for approximately 60% of the maximum total sediment transport which occurred at the breaking point. Unfortunately, this cannot be confirmed with the data since the contributions of bed and suspended load cannot be separated in the laboratory experiment. The location of the breaking point was correctly estimated by the wave model and generally was between the initial and final measured location of the breaking point.

(2) Coarse Sediment

Computation results for Cases B-215, B-225 and B-234 where $D_s = 0.7$ mm are shown in Fig. 5(b). When compared with measurements of Watanabe *et al.* (1980), it can be seen that the computed beach deformation and net sediment transport rates are also consistent. The computed sediment transport was onshore-directed which is consistent with those computed by Watanabe *et al.* (1980). Watanabe *et al.* (1980) noted that the bed load was predominant in cases where $D_s = 0.7$ mm. At this sediment size, the computations in this study still indicate the predominance of the suspended sediment. This renders inconclusive the investigation on whether the present sediment transport model can simulate properly the proportion of bed load and suspended sediment transports.

3.3. 3-D beach deformation

In a 3-D beach deformation laboratory experiment, Watanabe *et al.* (1986)[20] measured the wave heights, currents, and beach deformation around a detached breakwater. Sand with a median grain diameter of 0.2 mm was placed on a 4 m long by 7.2 m wide wave basin with an initial slope of $\tan\beta = 1/20$. A 1.5 m long and 0.5 m high model detached breakwater was placed parallel and 1.8 m offshore from the initial shoreline. Monochromatic waves with period and wave height $T = 0.87$ s and $H_i = 4.5$ cm respectively were incident normal to the initial shoreline. The bottom topography was measured at $t = 0{:}00$, 2:37, 5:05 and 6:55 (hr:min). The location of the breaker line was determined from overhead photographs taken near the middle of each time duration while the wave height and current fields were measured from $t = 0{:}00$ to 2:37, $t = 2{:}37$ to 5:05, and $t = 5{:}05$ to 6:55.

To verify the wave-current model performance under steeper bottom slopes and to verify the 3-D beach deformation model, numerical results were compared with measurements from this experiment. Two-dimensional numerical computations on a half-width of the wave basin were done. The uniform grid spacing was $\Delta x = \Delta y = 4$ cm, the computation time step was $\Delta t = 0.035$ s, and the bottom friction coefficient was estimated from the Jonsson (1966) friction factor formula. The incident boundary was set as an open boundary while the adjacent side boundaries were fully reflecting boundaries.

(1) Breaker Line

The computed breaker line location at $t = 0{:}00$ is shown in Fig. 6 taken at quasi-steady state that was achieved after 40 wave periods. In Fig. 6, it can be seen that the general location of the computed breaker line agrees with the measurements of Watanabe *et al.* (1986). Simulation by the present wave-current model was particularly good in the region behind the breakwater. This confirmed the applicability of the 2-D wave breaking criterion in a predominantly 2-D wave field.

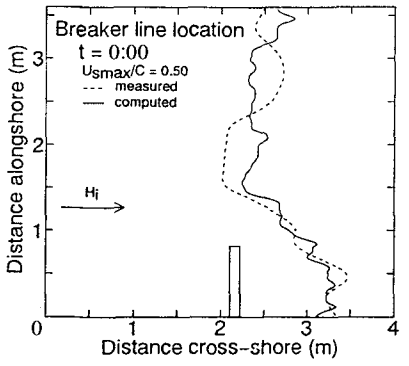

Figure 6 Comparison of breaker line location.

(2) Beach Deformation

Equations (10a) and (10b) were used to estimate the 2-D sediment transport based on the computed 2-D velocity field. The parameters used in Eqs. (10a) and (10b) were $\alpha_B = 1.0$, $a = 0.5$, $b = 1.0$, $\alpha_S = 3.5$, $p = 1.0$, and $\Psi_c = 0$. These values are similar to those used in 2-D beach deformation in the previous section. Equation (12) was then applied to calculate the 3-D beach deformation. The time step in the beach deformation computation was estimated by Eq. (13) with $\varepsilon = 4.0$.

The first 2-D wave-current computation followed by the first 3-D beach deformation computation gave results that were compared with measurements during the period $t = 0{:}00$ to 2:37 (hr:min). Using the newly computed beach topography at $t = 2{:}37$, the second 2-D wave-current computation followed by the second 3-D beach deformation computation were made and results were compared with measurements during the period $t = 2{:}37$ to 5:05.

The swash zone sediment transport was found to have been largely overestimated by the model as was discussed in 2-D beach deformation modeling. Hence, the sediment transport vector in the swash zone was linearly interpolated between those at the still water shoreline and maximum beach run-up point. The computed beach topographies are shown in Figs. 7(a) and 7(b). Compared with the laboratory measurements, it can be seen that the accretion behind the breakwater was simulated well. The alternate pattern of erosion and accretion in front of the breakwater was also simulated as well as the erosion at the tip of the breakwater. Some discrepancies still exist particularly at the region beyond the tip of the breakwater where the measured erosion was simulated at about 1 m onshore. When the computed and measured breaker line locations are compared, it can be observed that in this region, the computed breaker line was located onshore by roughly the same amount. This may explain the discrepancies in this region. This is further reinforced by the fact that both the measured and computed breaker lines are located along the steepest change in their respective bottom topographies. Moreover, the instantaneous near-bottom velocity may not have been estimated accurately in the region.

Comparing with results from the simple sediment transport model by Kabiling and Sato (1993), the present model simulated the beach topography change due to asymmetric nonlinear waves in the region bounded by $x > 2.0$ m and $y > 1.5$ m where x is the cross-shore distance from the incident boundary and y is the alongshore distance. In this region, erosion was simulated in the offshore side of the breaker line while accretion was simulated on the onshore side of the breaker line. In general, the measurements were qualitatively simulated by the present model and computations are consistent in magnitude particularly in the region located behind the breakwater.

(3) Wave Height and Nearshore Currents

The wave height and currents computed from the bottom topography at $t = 2{:}37$are shown in Figs. 8 and 9 respectively. These figures show results from computations started from still water conditions. The currents are the time average of the computed velocity field over one wave period. Agreement with measurements was improved over those presented by Kabiling and Sato (1993). The

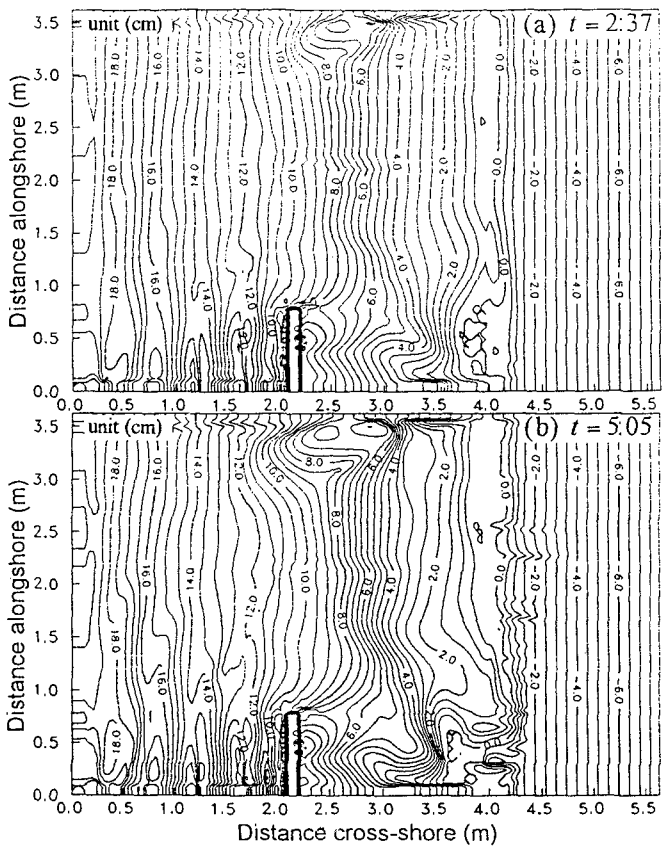

Figure 7 Computed beach topographies.

computed wave height shown in Fig. 8 exhibits an overall agreement with the measured wave height particularly in the surf zone. This can be observed by comparing Fig. 8 with Fig. 5.10 in Horikawa (1988)[3]. The nearshore circulation pattern behind the breakwater was simulated well by the present model as seen upon comparison of Fig. 9 with Fig. 5.10 in Horikawa (1988). The computed current magnitude was found to be consistent with the observed nearshore circulation pattern.

4. CONCLUSIONS

A two-dimensional nonlinear dispersive wave-current model was presented on the basis of the Boussinesq equations. The wave breaking criterion that is based on the ratio of water particle velocity at the surface of the wave crest to the wave celerity was found to accurately predict the breaker line location for a three-dimensional wave field. The correction terms that were introduced into the momentum equations were found to sufficiently simulate the wave decay caused by the

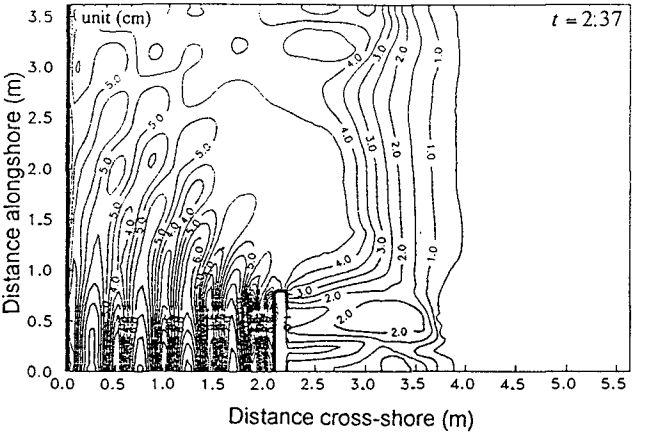

Figure 8 Computed wave height after initial beach topography change.

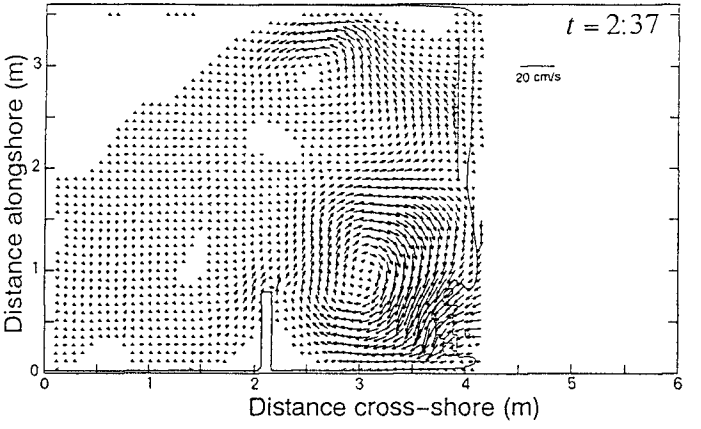

Figure 9 Computed currents after initial beach topography change.

momentum mixing and strong turbulence at the front face of the breaking wave. The wave set-up and set-down as well as the nearshore current have been simultaneously simulated by the model. The temporal variation of water surface elevation and near-bottom velocity was accurately estimated outside the surf zone. The accuracy of the estimation in the surf zone was slightly impaired. This can be caused by the use of a constant eddy viscosity during one wave period, the limited accuracy of the Boussinesq theory to weakly nonlinear and weakly dispersive waves, and by the assumption of a nearly horizontal bottom.

Beach evolution around a detached breakwater was estimated on the basis of the computed wave-current field. There was a general agreement and consistency with laboratory data of the 3-D beach deformation simulation result. The accretion behind the breakwater was simulated. The present sediment transport model was found to simulate surf zone sediment transport in the cross- shore and longshore directions including that caused by asymmetric wave motion. However, the present model was still seen to be unable to simulate the sediment transport in the swash zone.

REFERENCES

[1] Abbott, M.B., A.D. McCowan and I.R. Warren (1984): Accuracy of short wave numerical models, *J. Hydraulic Eng.*, Vol. 110, No. 10, pp. 1287-1301.

[2] Bailard, J.A. (1981): An energetics total load sediment transport model for a plane sloping beach, *J. Geophys. Res.*, Vol. 86, No. C11, pp. 10938-10954.

[3] Horikawa, K., Ed. (1988): *Nearshore Dynamics and Coastal Processes*, University of Tokyo Press, p. 311.

[4] Isobe, M. (1986): A parabolic equation model for transformation of regular waves due to refraction, diffraction and breaking, *Coastal Eng. in Japan*, Vol. 30, No. 1, pp. 33-47.

[5] Iwasaki, T. and A. Mano (1979): Numerical computations of two-dimensional run-ups of tsunamis due to Eulerian description, *Proc. 26th Japanese Conf. Coastal Eng.*, pp. 70-74 *(in Japanese).*

[6] Jonsson, I.G. (1966): Wave boundary layers and friction factors, *Proc. 10th Int. Conf. Coastal Eng.*, pp. 127-148.

[7] Kabiling, M. B. and S. Sato (1993): Two-dimensional nonlinear dispersive wave-current model and three-dimensional beach deformation model, *Coastal Eng. in Japan*, Vol. 36, No. 2, pp. 195-212.

[8] Karambas, T.V. and C. Koutitas (1992): A breaking wave propagation model based on the Boussinesq equations, *Coastal Eng.*, Vol. 18, pp. 1-19.

[9] Longuet-Higgins, M.S. (1970): Longshore currents generated by obliquely incident sea waves, *J. Geophys. Res.*, Vol. 75, No. 33, pp. 6778-6801.

[10] Madsen, P.A. and I.R. Warren (1984): Performance of a numerical short-wave model, *Coastal Eng.*, Vol. 8, pp. 73-93.

[11] Madsen, P.A., R. Murray and O.R. Sørensen (1991): A new form of the Boussinesq equations with improved linear dispersion characteristics, *Coastal Eng.*, Vol. 15, pp. 371-388.

[12] Maruyama, K. and T. Shimizu (1986): Simulation model for wave deformation considering interaction of waves and a beach, *Proc. 33rd Japanese Conf. Coastal Eng.*, pp. 109-113 *(in Japanese).*

[13] McCowan, A.D. (1987): The range of application of Boussinesq type numerical short wave models, *Proc. 22nd IAHR Cong.*, pp. 378-384.

[14] Sato, S., M. Fukuhama and K. Horikawa (1988): Measurements of near-bottom velocities in random waves on a constant slope, *Coastal Eng. in Japan*, Vol. 31, No. 2, pp. 219-229.

[15] Sato, S., M. Kabiling and H. Suzuki (1992): Prediction of near-bottom velocity history by a nonlinear dispersive wave model, *Coastal Eng. in Japan*, Vol. 35, No. 1, pp. 68-82.

[16] Schäffer, H.A., R. Deigaard and P. Madsen (1992): A two-dimensional surf zone model based on the Boussinesq equations, *Proc. 23rd Int. Conf. Coastal Eng.*, pp. 576-589.

[17] Shuto, N. (1974): Nonlinear long waves in a channel of variable section, *Coastal Eng. in Japan*, Vol. 17, pp. 1-12.

[18] Sunamura, T. and K. Horikawa (1974): Two-dimensional beach transformation due to waves, *Proc. 14th Int. Conf. Coastal Eng.*, pp. 920-938.

[19] Watanabe, A., Y. Riho and K. Horikawa (1980): Beach profiles and on-offshore sediment transport, *Proc. 16th Int. Conf. Coastal Eng.*, pp. 1106-1121.

[20] Watanabe, A., K. Maruyama, T. Shimizu and T. Sakakiyama (1986): Numerical prediction model of three-dimensional beach deformation around a structure, *Coastal Eng. in Japan*, Vol. 29, pp. 179-194.

[21] Watanabe, A. and M. Dibajnia (1988): A numerical model of wave deformation in surf zone, *Proc. 21st Int. Conf. Coastal Eng.*, pp. 578-587.